Structural, Morphological, Thermal, and Conductivity Studies of Magnesium Ion Conducting P(VdF-HFP)-Based Solid Polymer Electrolytes with Good Prospects

S. Ramesh, Soon-Chien Lu

Department of Mechanical and Material Engineering, Faculty of Engineering and Science, Universiti Tunku Abdul Rahman, Setapak, 53300 Kuala Lumpur, Malaysia

Received 10 September 2009; accepted 25 December 2009
DOI 10.1002/app.32051
Published online 6 April 2010 in Wiley InterScience (www.interscience.wiley.com).

ABSTRACT: Solid polymer electrolyte (SPE) system purely based on poly(vinylidenefluoride-hexafluoropropylene) [P(VdF-HFP)] and magnesium trifluoromethanesulfonate (MgTf) has been synthesized via solution-casting technique with acetone as solvent. Various instruments have been used to examine the structural, morphological, and thermal behaviors of the samples. X-ray diffraction (XRD), horizontal attenuated total reflectance-Fourier transform infrared spectroscopy (HATR-FTIR) and differential scanning calorimetry (DSC) are utilized to study the conversion of crystalline to amorphous nature in the copolymer. The crystallinity of copolymer matrix has been shown to be greatly affected by incorporation of MgTf, even with low concentration and absence of plasticisers. Scanning electron microscopy (SEM), photoluminescence spectroscopy (PL), and AC impedance spectroscopy further corroborate the findings. FTIR spectra suggest complexation has occurred between the constituents in these SPEs. Thermogravimetric analysis (TGA) and DSC thermograms show some improvements in thermal behaviors upon the addition of MgTf.
 J Appl Polym Sci 117: 2050–2058, 2010

Key words: solid polymer electrolytes; poly (vinylidenefluoride-hexafluoropropylene); magnesium trifluoromethanesulfonate; structural studies; morphological studies; thermal studies

INTRODUCTION

Solid polymer electrolytes (SPEs) fulfill the requirements and overcome the limitations of conventional liquid electrolytes by addressing drawbacks such as electrolyte leakage, flammable organic solvent, and electrolytic degradation of electrolytes.[1] When compared with gel polymer electrolytes (GPEs), SPEs are typically less reactive toward the electrodes. Additionally, they provide higher safety, prevent the build-up of internal pressure during battery cycling and can be designed in many desirable sizes and shapes.[2] In a rechargeable battery, SPE serves as both the separator to prevent the electrodes from coming into physical contact, and more essentially, as the ionic conductor.[3]

High ionic conductivity, adequate chemical and mechanical strength, extended thermal stability, and low price are the favorable characteristics of polymer electrolyte membranes.[3] Among the various types of polymers being studied, poly(vinylidenefluoride-*co*-hexafluoropropylene) [P(VdF-HFP)]-based polymer electrolytes show relatively high ionic conductivities at ambient temperature, and it has been successfully used as the quasi-solid state materials in combination with room temperature ionic liquids showing good conversion efficiencies.[4] It is semi-crystalline and a chemically resistant copolymer with excellent mechanical strength and relatively high dielectric constants. High-dielectric constant materials have received growing interest in recent years as they are attractive as potential materials for various applications including gate dielectrics, high charge-storage capacitor, and electroactive materials.[5] Besides, it also exhibits a lower glass transition temperature, a lower melting temperature, and a higher solubility in organic solvents.[6] All these credits make it an ideal candidate as polymer host for SPEs.

Many solid polymer electrolytes are focused mainly on alkali metal salt systems, with particular attention given to lithium. Out of the metals that have not been so widely studies, magnesium salts are of considerable interest because of the divalent charge and the 2 : 1 anion to cation ratio. It is expected that divalent species with stronger coulomb interaction bears stronger structural and bonding implications in the formation of SPE and appears as an attractive candidate.[7] Besides, investigations on rechargeable magnesium batteries are interesting

Correspondence to: S. Ramesh (ramesh@utar.edu.my).
Contract grant sponsor: Malaysia Toray Science Foundation (MTSF), UTAR Research Fund (UTARRF).

on three accounts in comparison with lithium batteries: (i) The ionic radii of Li^+ and Mg^{2+} are 68 and 65 pm, respectively, which are comparable in magnitude, (ii) magnesium metal is more stable than lithium and can be handled safely in oxygen and humid atmospheres, and (iii) the global raw material resources of magnesium are plentiful. Owing to these merits, investigations on electrochemistry of magnesium-based rechargeable battery systems assume significant importance.[8]

In this work, the effect of magnesium trifluoromethanesulfonate (MgTf) salt in structural, morphological, and thermal behaviors in P(VdF-HFP)-based polymer electrolytes have been evaluated. To achieve the stated objectives, various common analyzes such as horizontal attenuated total reflectance-Fourier transform infrared spectroscopy (HATR-FTIR), X-ray diffraction (XRD), scanning electron microscopy (SEM), photoluminescence spectroscopy (PL), thermogravimetric analysis (TGA), differential scanning calorimetry (DSC), and AC impedance spectroscopy are used.

EXPERIMENTAL

Materials

Poly(vinylidenefluoride-hexafluoropropylene) [P(VdF-HFP)] with average M_w = 455,000 was obtained from Sigma-Aldrich. Magnesium trifluoromethanesulfonate (MgTf) salt was obtained from Acros and dried at 100°C for 1 h to eliminate trace amounts of water in the material, before the preparation of solid polymer electrolytes (SPEs). Acetone of AR grade was obtained from J. T. Baker.

Preparation of thin films

Several polymer electrolyte complexes were prepared as in the compositions according to its weight ratio of polymer to lithium salt, which are 90/10, 25/75, and 60/40, respectively. The thin films were prepared by solution-casting technique with acetone as solvent. The mixture was casted on a Petri dish and allowed to evaporate slowly inside a fume hood. This procedure yields mechanically stable and free standing films. The completeness of acetone solvent removal can be checked by HATR-FTIR spectroscopy. The thickness of the films was measured using a micrometer screw gage.

Instrumentation

The HATR-FTIR studies was carried out using Perkin-Elmer FTIR spectrometer spectrum RX1 with horizontal attenuated total reflection accessory in the wave region between 1800 cm^{-1} and 650 cm^{-1}, with resolution 4 cm^{-1}. Also, there were no signs of a carbonyl band from residual acetone around 1700 cm^{-1}, suggesting complete removal of acetone as solvent.

The XRD patterns were analyzed using Siemens D-5000 Diffraction System using Cu-K_α radiation with the wavelength of 1.5406 Å. The diffraction pattern was recorded at room temperature for the Bragg angles (2θ) varying from 10° to 80°.

Those selected SPEs were then subjected to SEM, with the model Leica S440. All the scanning electron micrographs share a common magnification factor of 5000.

Thermogravimetric analysis (TGA) was performed with a Mettler Toledo analyzer that consists of a TGA/SDTA851^e main unit and STARe software with 10°C min^{-1} heat rate between 30°C and 500°C under a nitrogen atmosphere.

Differential scanning calorimetry (DSC) was also performed with Mettler Toledo analyzer that consists of a DSC823^e main unit and STARe software. Approximately 2 mg of sample was sealed in the standard 40 μL aluminum pan. The sample was heated sequentially from 30°C to 100°C, remained for 1 min, and then cooled down to 30°C to eliminate the trace amount of water absorbed into the sample. After that, it was reheated up to 200°C and again cooled down to 30°C. The heat rate used was 10 and −10°C min^{-1} for heating and cooling cycle, respectively. All measurements were recorded under nitrogen atmosphere.

Perkin-Elmer LS55 luminescence spectrometer is used for photoluminescence measurements. The sample holder was placed 60° against the excitation wavelength. The excitation and emission wavelengths have been set at 280 nm and 360 nm, respectively.

A HIOKI 3532-50 LCR Hi-Tester was used to perform the impedance measurements for each SPE over the frequency range of 50 Hz to 1 MHz. The equation $\sigma = l/R_bA$ is used to calculate the ionic conductivity of thin film sample, where σ is conductivity in S cm^{-1}, l is thickness of thin film sample in cm, R_b is bulk resistance in Ω obtained from Cole-Cole impedance plot, and A is surface area of stainless steel blocking electrodes in cm^2.

RESULTS AND DISCUSSION

Horizontal attenuated total reflectance-Fourier transform infrared spectroscopy

Fourier transform infrared (FTIR) spectroscopy is a vital part in the investigation of interactions between macromolecules and ions taking place in polymer electrolytes. SPE's bands in these FTIR spectra vary as a result of different compositions and occurrence of complexation or interaction between various

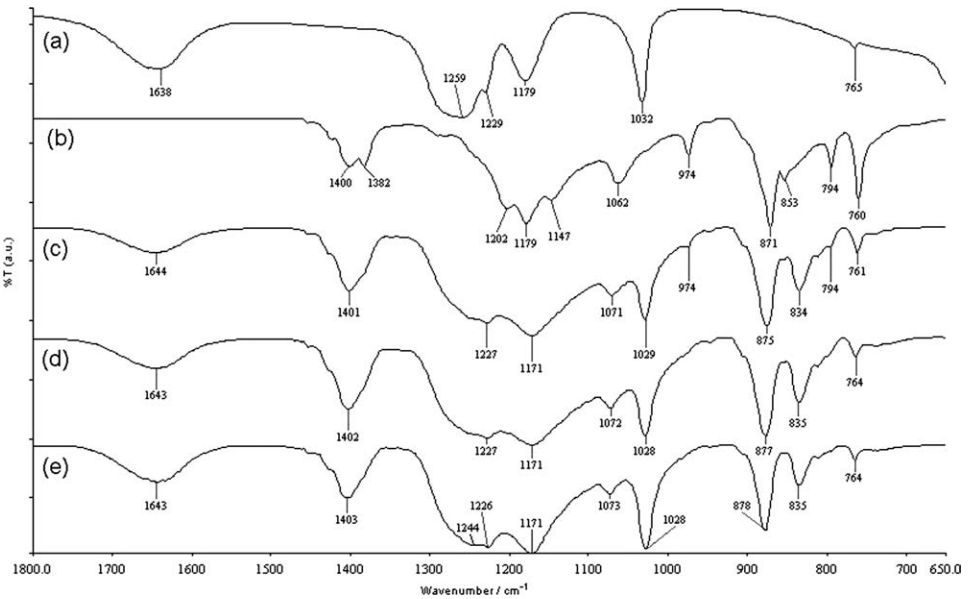

Figure 1 HATR-FTIR spectra of (a) MgTf salt, (b) pure P(VdF-HFP), (c) MT10, (d) MT25, and (e) MT40 in transmittance mode.

constituents. It is applicable in determining the occurrence of complexation in crystalline or amorphous phase as well.[9] With the help of horizontal attenuated total reflectance (HATR) accessory, FTIR spectra can be obtained directly from the resulting solid polymer electrolyte thin films samples of this work, without redissolving them with acetone. FTIR spectra of LiTf salt, pure P(VdF-HFP), MT10, MT25, and MT40 are shown in Figure 1. All HATR-FTIR spectra are recorded in transmittance mode. Some of the possible band assignments for P(VdF-HFP) and MgTf have already been reported in literature[10–13] and listed in Table I.

The bands mentioned in Table I are observable in Figure 1(a,b). For MgTf, symmetrical stretching of CF_3 is observed at 765 cm^{-1}, symmetrical stretching of SO_3 at 1032 cm^{-1}, asymmetrical stretching of SO_3 at 1179 cm^{-1} and 1259 cm^{-1}, symmetrical vibration of CF_3 at 1229 cm^{-1}, and characteristic peak of Tf^- anion at 1638 cm^{-1}. On the other hand, for P(VdF-HFP), α-phase of PVdF is observed at 760, 853, and 974 cm^{-1}, CF_3 stretching at 794 cm^{-1}, amorphous region at 871 cm^{-1}, C—C skeletal vibration at 1147 cm^{-1}, —CF_2— stretching at 1147 cm^{-1}, symmetrical stretching of —CF_3 at 1179 cm^{-1}, asymmetrical stretching of —CF_2— at 1203 cm^{-1}, and —C—F— stretching at 1382 cm^{-1} and 1400 cm^{-1}.

In HATR-FTIR spectrum of sample MT10 in Figure 1(c), which contains P(VdF-HFP) : MgTf (90 : 10), it is observed that there is formation of a new peak at 834 cm^{-1}. This can be assigned to band that attributes to newly formed amorphous region of P(VdF-HFP).[14] There are several peaks that have visible decrease in intensity, such as asymmetrical stretching of SO_3 at 1259 cm^{-1} and characteristic peak of Tf^- anion at 1638 cm^{-1} from Figure 1(a), and also α-phase of PVdF at 760 cm^{-1} and 974 cm^{-1}, together with CF_3 stretching at 794 cm^{-1} from Figure 1(b). However, there are more apparent changes observed from Figure 1(b,c). The bands at 1147, 1179, and 1202 cm^{-1} in Figure 1(b) merge to form a single peak at 1171 cm^{-1} in Figure 1(c). The same observation happens for 1382 cm^{-1} and 1400 cm^{-1} in Figure 1(b). The two peaks also merge to form another single peak at 1401 cm^{-1} in Figure 1(c).

TABLE I
Possible Assignments of Transmittance Bands in HATR-FTIR Spectra of Pure P(VdF-HFP) and MgTf

Compound	Wavenumber (cm^{-1})	Possible assignment
MgTf	765	Symmetrical deformation mode of CF_3
	1032	Symmetrical stretching of SO_3
	1179, 1259	Asymmetrical stretching of SO_3
	1229	Symmetrical vibration of CF_3
	1638	Characteristic peak of Tf^-
P(VdF-HFP)	760, 853, 974	α-phase
	794	CF_3 stretching
	871	Amorphous region
	1062	C—C skeletal vibration
	1147	—CF_2— stretching
	1179	Symmetrical stretching of —CF_3
	1202	Asymmetrical stretching of —CF_2—
	1382, 1400	—C—F— stretching

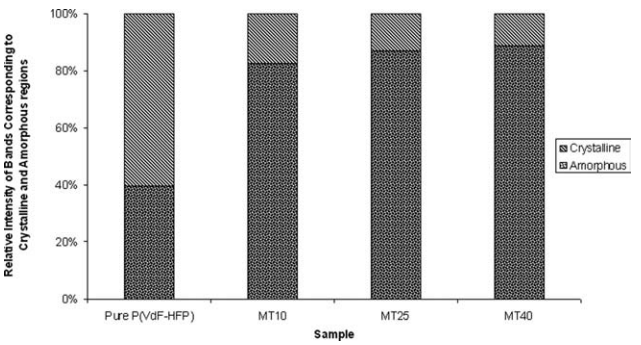

Figure 2 Comparison of relative intensity of bands corresponding to crystalline and amorphous regions of pure P(VdF-HFP), MT10, MT25, and MT40 shown in HATR-FTIR spectra.

When the concentration of MgTf increases from low, intermediate to high (10, 25, and 40 wt %, respectively), there are two other observable changes in the HATR-FTIR spectra as well. The intensities of bands at 794, 853, and 974 cm^{-1} decrease to unnoticeable, whereas bands at 834 and 875 cm^{-1} increase to become more prominent. The former three bands correspond to the α-phase of PVdF, which is actually the crystalline region of the copolymer, whereas the latter two bands correspond to the amorphous region of the copolymer. The relative intensity of these two groups of bands that are obtained from the calculation of computer program software "Spectrum" is shown in Figure 2 for pure P(VdF-HFP), MT10, MT25, and MT40 samples. As seen, the MgTf loading leads to an abrupt decrease of crystallinity and followed by slighter increase of amorphosity with increasing amount of MgTf. However, this only serves as a representation for the sake of comparison, rather than the actual ratio of crystalline to amorphous region. Other bands such as 1029, 1249, and 1644 cm^{-1} have increased in intensity, when the concentration of MgTf is increased.

The disappearance and shifting of some bands, formation of new peaks, and changes in intensity of the peaks in the HATR-FTIR spectra of SPEs suggest that some extent of co-ordination or complexation has occurred between the constituents in these SPEs,[15] namely, P(VdF-HFP) and MgTf. In summary, these observations establish the complexation of P(VdF-HFP) with MgTf.

X-ray diffractometry analysis

Besides FTIR, XRD analysis is one of the most common ways to investigate the occurrence of complexation between polymer host and dopant salt in polymer electrolytes.[16] XRD patterns of pure P(VdF-HFP) thin film recast from its acetone solution, P(VdF-HFP)/MgTf solid polymer electrolyte (SPE) thins films with 10, 25, and 40 wt % are shown in Figure 3.

For pure P(VdF-HFP), four peaks are found at $2\theta = 18.0$, 20.0, 26.9, and 38.8°, which correspond well with the characteristic peaks at $2\theta = 18.2$, 20, 26.6, and 38° for crystalline pure poly(vinylidene) (PVdF) reported in literature.[17,18] This suggests the coexistence of multiphase system having crystalline PVdF and amorphous PHFP regions. This can be a confirmation of the partial crystallization of PVdF units in the copolymer and gives a semi-crystalline structure of P(VdF-HFP).[19]

When 10 wt % of MgTf is incorporated into the pure polymer, it causes a shift in the P(VdF-HFP) peak at $2\theta = 20.0°$ to 20.7°. The behavior demonstrates that complexation has occurred between the magnesium salt and the polymer.[20] As more MgTf is added, the intensity of peak at $2\theta = 20.0°$ is gradually reduced. This implies that the salt has disrupted the crystalline region of (PVdF-HFP) and increased the amorphous region.

The increasing domain of amorphous region in the samples is evident from the broadening of the crystalline reflections at $2\theta = 38.8°$.[21] This suggests either the formation of smaller crystallites in the semi-crystalline PVdF or a less-ordered structure of the salt containing system, which leads to reconstruction of amorphous nature.[22] The amorphous domain of polymer electrolytes allows greater diffusion in accordance with high ionic conductivity, which can be obtained in amorphous membranes that have a fully flexible backbone.[23] Generally, a decrease in the crystalline region effectively increases the flexibility of the polymeric backbone, and thus promotes better ionic transport.[24]

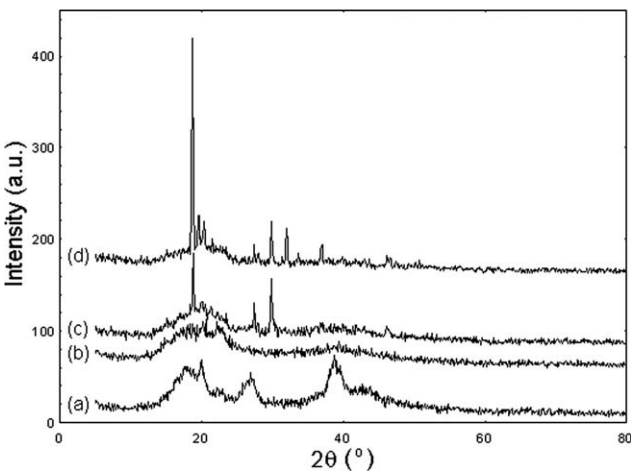

Figure 3 X-ray Diffractograms of (a) pure P(VdF-HFP), (b) MT10, (c) MT25, and (d) MT40.

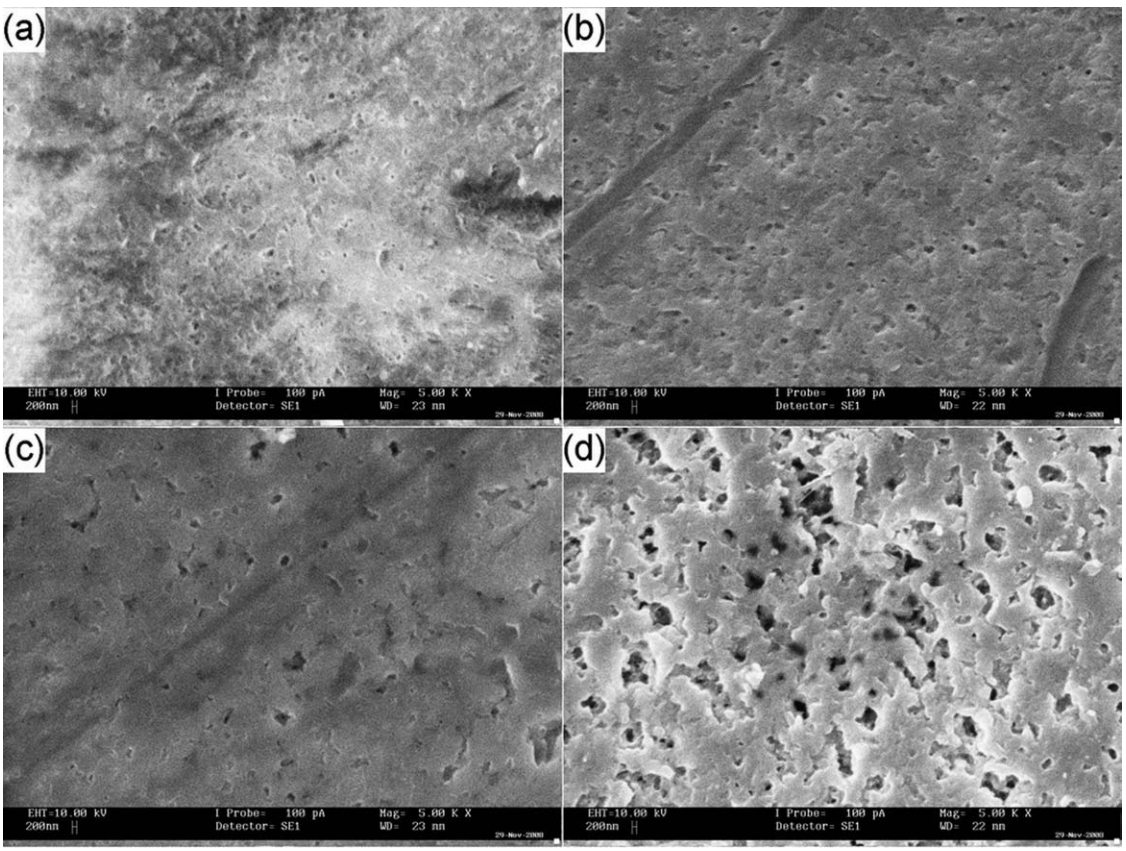

Figure 4 Scanning electron micrographs of (a) pure P(VdF-HFP), samples (b) MT10, (c) MT25, and (d) MT40 with magnification factor of 5000.

On the other hand, Figure 3(c,d) show a few new peaks at $2\theta = 18.7$, 27.4, 29.8, 32.0, 33.8, and 37.0°, appear above the salt concentration of 25 wt %. This indicates that there is certain amount of free salt, which does not complex with polymer because of the excess amount of it. These peaks may also arise from large ion clusters that are formed by strong interaction of ions and the ordering of large ion clusters, concerning with ion percolation paths, is accelerated with salt concentration.[25]

Scanning electron microscopy

Depending on the type and amount of salt present in the polymer matrix, the morphology of the polymer electrolyte will vary and greatly influence its properties. Morphological examination of this study is carried out to study the phase morphology changes of the pure polymer and the resulting solid polymer-electrolyte thin films, after the addition of magnesium salt. Scanning electron micrographs of pure P(VdF-HFP), samples MT10, MT25, and MT40 have been presented in Figure 4.

Very distinguishable changes can be observed from pure P(VdF-HFP), to low, intermediate and high concentrations of MgTf. Pure P(VdF-HFP) shows normal porous surface with uniform small pore size. The morphology changes, as soon as 10 wt % of MgTf is incorporated into the polymer, to become having less number of pore. It also starts to show some kind of layered feature. When the magnesium salt concentration reaches 25 wt %, the morphology follows the observation in MT10, only with even lesser amount of pore and greater pore size. When higher amount of magnesium salt is added into the polymer, say 40 wt % of MgTf in this case, the morphology changes drastically to become significantly more layered and even greater pore size. These features are very similar to those reported in literature.[10]

This type of morphology in sample MT40 has been observed before and designated to be spheroidal.[6] An open pore structure of the polymer electrolyte matrix is essential for ionic conductivity across the thin film.[26] This type of open porous structure provides enough channels for the migration of ions, accounting for better ionic conductivity.[27]

Photoluminescence (PL) spectroscopy

As discussed earlier, ionic conductivity can be related to ion mobility, which is strongly associated with amorphosity. In samples with high amorphous nature, the conducting ions within that sample

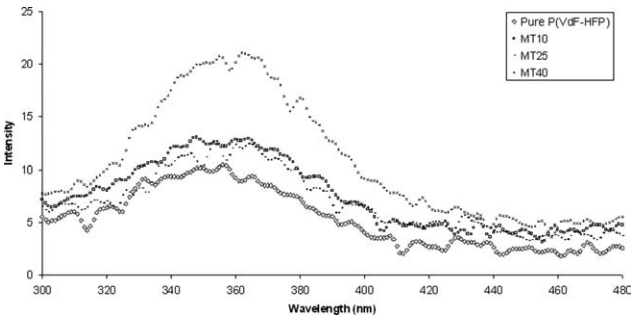

Figure 5 Photoluminescence emission spectra of pure P(VdF-HFP) (◆), MT10 (□), MT25 (-), and MT40 (×) with excitation (λ_{exc}) at 280 nm.

should have better mobility to give greater ionic conductivity. It is generally accepted that in the conventional polymer electrolyte, conducting cations are coordinated by strongly electron-withdrawing constituents, such as fluorine in P(VdF-HFP) backbone. Thus, ion conduction is strongly coupled with segmental motions of the polymer matrix, which are closely associated with the local free volume and local viscosity around the charge-transporting ions.[28] Fluorescence studies can be used to provide information on local viscosity effects in SPEs. This technique can also detect structural alterations in the local environment and it has been used to study the structural, conformational, and dynamic properties of polymer systems.[29]

Typical fluorescence emission and excitation spectra of pure P(VdF-HFP), MT10, MT25, and MT40 are shown in Figures 5 and 6, respectively. The results are very similar to that reported in literature.[30] There is no distinctive change in shape of spectra upon the addition of magnesium salt. However, it can be clearly observed that as the content of magnesium salt increases the intensity also increases. SPE with the highest content of MgTf, MT40, exhibits a higher intensity than other SPEs. This suggests the higher degree of free ionic motion, or simply ion mobility, is observed when greater amount of magnesium salt is incorporated with P(VdF-HFP). The enhancement of ion mobility can be attributed to the addition of MgTf that disrupts the crystalline phase of P(VdF-HFP) and restructures it to amorphous.

Thermogravimetric analysis (TGA)

The weight loss of the pure P(VdF-HFP), together with samples MT10, MT25, and MT40 have been subjected to thermogravimetric analysis (TGA) under nitrogen atmosphere, to examine their thermal stability, which is important from the industrial point of view. The TGA thermograms in Figure 7 show that all the samples are thermally stable up to 380°C. This is highly desirable for its potential applications in electrochemical devices.

Minor weight losses are found in almost all samples during initial heating. This is most likely due to the moisture absorption into the thin films given that the magnesium salts are quite sensitive to moisture.[10] More interestingly, the initial weight losses of MT25 and MT40 do not stop until ~150°C, which can be attributed to the greater interaction between the divalent magnesium ions and the moisture/residual solvent molecules. Volatilization of monomers and oligomers adsorbed in the polymer matrix can also be responsible for these initial weight losses.[20]

Thermal data such as weight loss percentages, decomposition temperatures, and onset temperatures of decomposition of pure P(VdF-HFP), MT10, MT25, and MT40 obtained from thermograms have been tabulated in Table II. From the table, it can be observed the weight loss percentage increases immediately upon the addition of MgTf. This can be due to the presence of Tf^- group, which can be burnt off easily as carbon oxides, sulfur oxides, and hydrogen fluoride, as compared with the polymer host and Mg^{2+} ions. However, the weight loss of MT10 only differs marginally when compared with that of pure P(VdF-HFP). This can be to the less interaction

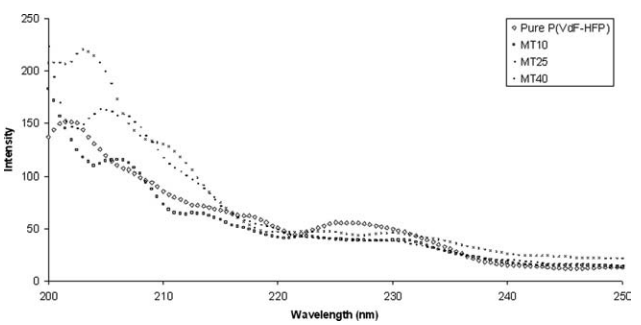

Figure 6 Photoluminescence excitation spectra of pure P(VdF-HFP) (◆), MT10 (□), MT25 (-), and MT40 (×) with emission (λ_{emn}) at 360 nm.

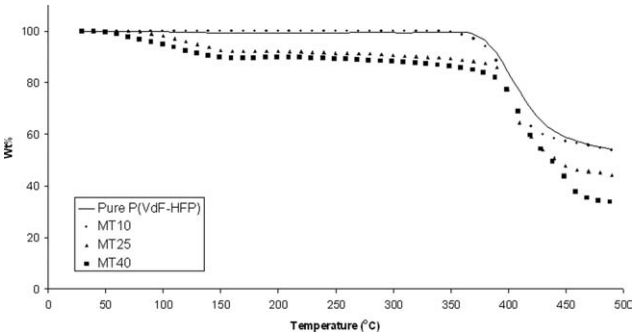

Figure 7 Normalized dynamic TGA thermograms of pure P(VdF-HFP) (-), samples MT10 (●), MT25 (▲), and MT40 (■) under nitrogen atmosphere.

TABLE II
Weight Loss Percentages, Decomposition Temperatures, and Onset Temperatures of Decomposition of Pure P(VdF-HFP), MT10, MT25, and MT40 Obtained from Normalized TGA Thermograms

Sample	% Weight loss (up to 500°C)	Decomposition temperature (T_D)	Onset temperature of decomposition
Pure P(VdF-HFP)	46.21%	405.94°C	384.74°C
MT10	46.81%	397.81°C	381.47°C
MT25	52.13%	401.39°C	392.20°C
MT40	62.87%	401.27°C	394.94°C

between the polymer host and magnesium salt, as the content of magnesium in MT10 is too low to cause significant disruption of crystallinity of the polymer. When the concentration increases, this effect starts to take place and causes high degree of ion dissociation. When magnesium salt is dissociated into Mg^{2+} and Tf^{-} ions, the latter is much susceptible to thermal degradation. The weight loss percentage drastically increases to 62.87% as 40 wt % of MgTf is added into the system.

On the contrary, the dissociated magnesium ions have caused other beneficial effects, which are the increments of onset temperatures of decomposition and decomposition temperatures. The onset temperature of decomposition of samples increases from about 380°C to 395°C, and slightly lesser extent for decomposition temperature, which increases from $\sim$ 398 to 401°C, upon the addition of MgTf. This can be related to the presence of higher level magnesium metal ions, which requires more energy to be thermally degraded. Although MT40 suffers from having the highest weight loss percentage, it is compensated with improved decomposition temperature and highest onset temperature of decomposition. The thermal stability of P(VdF-HFP)-based solid polymer electrolytes, in this study, is sufficient to be applied in the fuel cells, which operate at above 100°C.[24]

Differential scanning calorimetry (DSC)

DSC techniques have been used widely to study phase transition of polymer electrolytes in order to correlate thermal information about the amorphous and crystalline phases with ionic conductivity.[31] The glass transition, melting, and crystallization temperatures together with thermal stability of the materials are all important parameters resulting from the microstructure and morphology of the system.[22] However, the glass transition temperatures have not been examined due to the limitation of the DSC instrument used. Figures 8 and 9 show the DSC thermograms of pure P(VdF-HFP), MT10, MT25, and MT40 in heating and cooling runs, respectively.

For the heating runs, the endothermic peak at 137°C in Figure 8(a) corresponds to the melting of

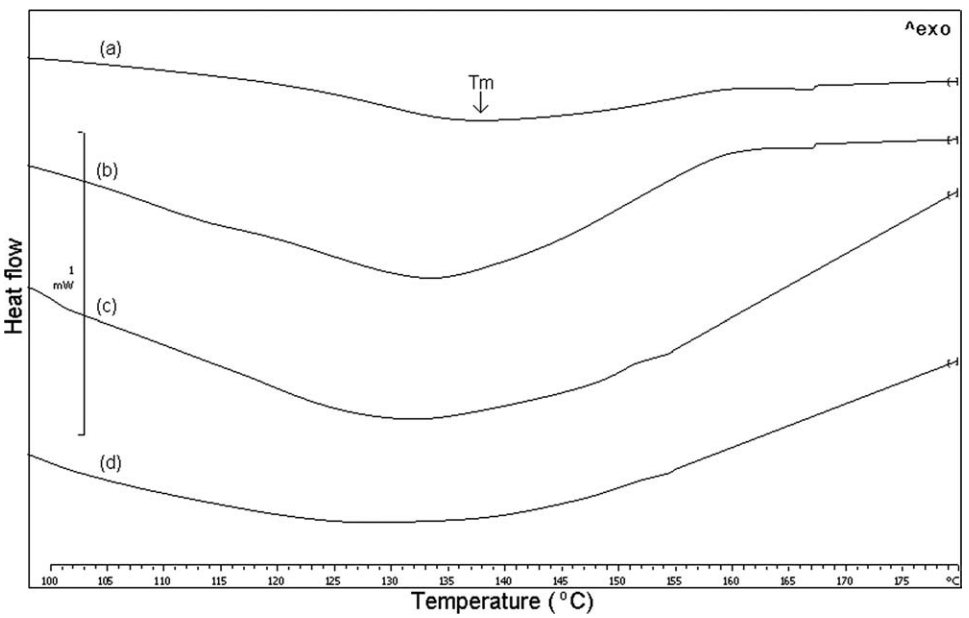

Figure 8 DSC thermograms of (a) pure P(VdF-HFP), (b) MT10, (c) MT25, and (d) MT40 in heating run.

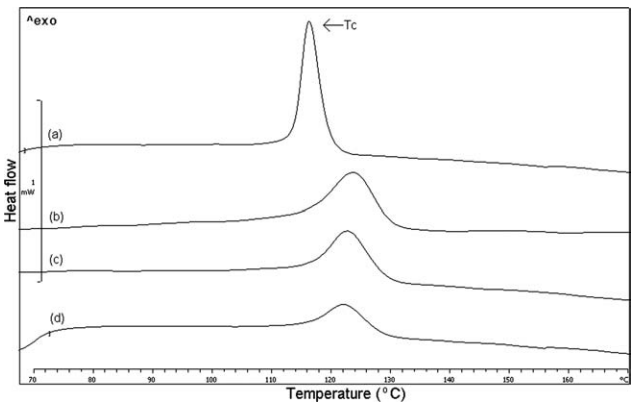

Figure 9 DSC thermograms of (a) pure P(VdF-HFP), (b) MT10, (c) MT25, and (d) MT40 in cooling run.

the copolymer P(VdF-HFP) SPE thin film, which is close to that reported in literature.[10] When concentration of MgTf increases, the samples exhibit lower melting temperatures than that of pure polymer, accompanied with broadening of melting peak, as shown in Figure 8. The variation of melting temperatures (T_M) and broadening of melting endotherms can be associated with the interaction between MgTf and polymer chains[11] or changes in PVdF crystal phase from dominant α-phase to coexistence of α-, β-, and γ-phase crystals.[32]

As for the cooling runs, the crystallization temperature appears at higher crystallization temperatures (T_C) upon the addition of MgTf in Figure 9, probably due to the sparsely distributed MgTf that plays the role of nucleating agent and of accelerating the crystal growth.[33] However, the crystallization exotherms in these samples shift slightly toward lower temperatures with increasing magnesium salt content, as the densely populated MgTf no longer promotes but rather inhibits the growth of polymer crystals to give delayed recrystallization.[34] The T_C occurring at lower temperature than T_M is typical for macromolecules.

Table III shows the calculated crystallinity (X_C) of same set of samples. Crystallinity (X_C) can be determined from the equation $X_C = \left(\frac{\Delta H_m}{\Delta H_m^0}\right) \times 100\%$ from the cooling DSC thermograms, where ΔH_m denotes the heat of fusion of sample and $\Delta H_{\mathrm{m}}^{\theta}$ as the reference heat of fusion of the crystalline α-PVdF, 104.7 J g^{-1}.[35] The area under the curve is getting smaller and smaller with increasing amount of MgTf. With the values calculated from the computer software, when the amount of lithium salt increases, crystallinity of the samples decreases, as shown in Table III. This result is commensurate with the findings of XRD and HATR-FTIR data discussed in previous sections. It is well-known that amorphous/crystalline nature affects the ionic conductivity of polymer electrolytes. As the complexation between the magnesium salt and polymer primarily takes place in amorphous region, the migration of ions can be promoted by the decrease of crystallinity of the polymer matrix, thus leading to higher ionic conductivity.[36]

TABLE III
Calculated Crystallinity of Pure P(VdF-HFP), MT10, MT25, and MT40

Sample	Crystallinity (X_C)
Pure P(VdF-HFP)	20.98%
MT10	14.91%
MT25	9.26%
MT40	6.63%

Ionic conductivity

To complete the investigation of SPE, ionic conductivity, which is the most important property of membranes, was also performed using AC impedance spectrometer at room temperature. Figure 10 depicts ionic conductivity of recast P(VdF-HFP), MT10, MT25, and MT40 at room temperature. Membrane recast from P(VdF-HFP) shows extremely low conductivity in the order of 10^{-11} S cm^{-1}. The abrupt jump of conductivity values from pure P(VdF-HFP) to MT10 is clearly due to availability of dopant salt in the system. However, this trend does not continue when higher amount of MgTf is doped into the system. The gradient of plots changes sharply to a much flatter one. This change of ionic conductivity enhancement rate suggests that it is caused by factors other than increasing amount of dopant salt in the system, which can be surmised as declining of crystallinity in P(VdF-HFP) as a result of MgTf salt incorporation. Results shown in Figure 10 indeed corroborate with all the discussions above, as ionic conductivity is closely related to polymer's crystallinity.

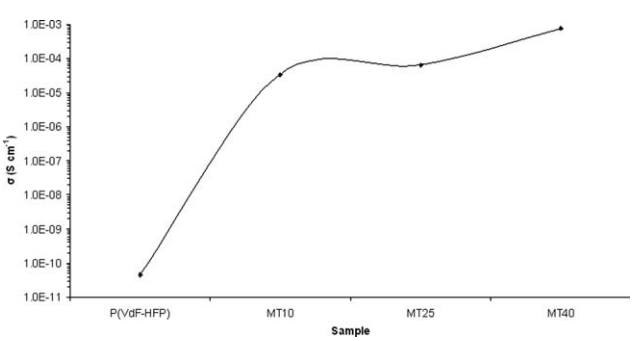

Figure 10 Ionic conductivity of P(VdF-HFP), MT10, MT25, and MT40 at room temperature.

CONCLUSIONS

A series of SPE system based on P(VdF-HFP) and MgTf that range from 10 to 40 wt % have been synthesized via solution casting technique with acetone as solvent. FTIR spectra reveal some disappearance and shifting of bands, changes in intensity, and formation of new peaks suggest that MgTf is well-dissociated within P(VdF-HFP) and complexation has occurred between the constituents in these SPEs. XRD, HATR-FTIR, and DSC data suggest that the incorporation of MgTf effectively reduces the degree of crystallinity in P(VdF-HFP)-based solid polymer electrolytes, even at low concentration. SEM, PL, and impedance spectrometer further corroborate the findings with the existence of spheroidal structure in the micrograph, achieving higher intensity in the PL spectrum and difference observed in ionic conductivity enhancement rate. This signifies that MgTf is successfully incorporated and complexed with P(VdF-HFP), which leads to the effective disruption of crystalline domain and gives rise to new P(VdF-HFP)/MgTf amorphous phase. TGA and DSC thermograms show improvements in decomposition temperature, onset temperature of decomposition, melting, and crystallization temperatures upon the addition of MgTf. This system has already shown good prospects even with only a polymer host and a magnesium salt. It is worthy to be further explored with incorporation of other additives, such as plasticisers, fillers, or ionic liquids.

References

1. Li, Y. X.; Yerian, J. A.; Khan, S. A.; Fedkiw, P. S. J Power Sources 2006, 161, 1288.
2. Song, J. Y.; Wang, Y. Y.; Wan, C. C. J Power Sources 1999, 77, 183.
3. Jacob, M. M. E.; Hackett, E.; Giannelis, E. P. J Mater Chem 2003, 13, 1.
4. Lee, K.-M.; Suryanarayanan, V.; Ho, K.-C. J Power Sources 2008, 185, 1605.
5. Lu, J.; Moon, K.-S.; Wong, C. P. J Mater Chem 2008, 18, 4821.
6. Elmer, A. M.; Wesslen, B.; Sommer-Larsen, P.; West, K.; Hassandera, H.; Jannasch, P. J Mater Chem 2003, 13, 2168.
7. Reddy, M. J.; Chu, P. P. Solid State Ionics 2002, 149, 115.
8. Kumar, G. G.; Munichandraiah, N. J Power Sources 2001, 102, 46.
9. Rajendran, S.; Uma, T. Mater Lett 2000, 44, 208.
10. Pandey, G. P.; Hashmi, S. A. J Power Sources 2009, 187, 627.
11. Li, Z. H.; Zhang, H. P.; Zhang, P.; Li, G. C.; Wu, Y. P.; Zhou, X. D. J Membr Sci 2008, 322, 416.
12. Suthanthiraraj, S. A.; Kumar, R.; Paul, B. J. Spectrochim Acta Part A 2009, 71, 2012.
13. Ramesh, S.; Chai, M. F. Mater Sci Eng B 2007, 139, 240.
14. Aravindan, V.; Vickraman, P.; Kumar, T. P. J Non-Cryst Solids 2008, 354, 3451.
15. Ramesh, S.; Lu, S.-C. J Power Sources 2008, 185, 1439.
16. Ramalingaiah, S.; Reddy, D. S.; Reddy, M. J.; Laxminarsaiah, E.; Rao, U. V. S. Mater Lett 1996, 29, 285.
17. Saikia, D.; Kumar, A. Electrochim Acta 2004, 49, 2581.
18. Saikia, D.; Chen-Yang, Y. W.; Chen, Y. T.; Li, Y. K.; Lin, S. I. Desalination 2008, 234, 24.
19. Stephan, A. M.; Nahm, K. S.; Kulandainathan, M. A.; Ravi, G.; Wilson, J. Eur Polym J 2006, 42, 1728.
20. Ramesh, S.; Arof, A. K. J Power Sources 2001, 99, 41.
21. Subban, R. H. Y.; Arof, A. K. J New Mater Electrochem Syst 2003, 6, 197.
22. Abbrent, S.; Plestil, J.; Hlavata, D.; Lindgren, J.; Tegenfeldt, J.; Wendsjö, Å. Polymer 2001, 42, 1407.
23. Subramania, A.; Kalyana Sundaram, N. T.; Priya, A. R. S.; Kumar, G. V. J Membr Sci 2007, 294, 8.
24. Kumar, G. G.; Kim, P.; Kim, A. R.; Nahm, K. S.; Elizabeth, R. N. Mater Chem Phys 2009, 115, 40.
25. Yoon, H.-K.; Chung, W.-S.; Jo, N.-J. Electrochim Acta 2004, 50, 289.
26. Aravindan, V.; Vickraman, P. Ionics 2007, 13, 277.
27. Li, G. C.; Zhang, P.; Zhang, H. P.; Yang, L. C.; Wu, Y. P. Electrochem Commun 2008, 10, 1883.
28. Park, U.-S.; Hong, Y.-J.; Oh, S. M. Electrochim Acta 1996, 41, 849.
29. Waldow, D. A.; Ediger, M. D.; Yamaguchi, Y.; Matsushita, Y.; Noda, I. Macromolecules 1991, 24, 3147.
30. Aravindan, V.; Vickraman, P. Mater Chem Phys 2009, 115, 251.
31. Silva, R. A.; Silva, G. G.; Moreira, R. L.; Pimenta, M. A. Phys Chem Chem Phys 2003, 5, 2424.
32. Sajkiewicz, P. Eur Polym J 1999, 35, 1581.
33. Kim, K. M.; Ryu, K. S.; Kang, S.-G.; Chang, S. H.; Chung, I. J. Macromol Chem Phys 2001, 202, 866.
34. Kim, K. M.; Ko, J. M.; Park, N.-G.; Ryu, K. S.; Chang, S. H. Solid State Ionics 2003, 161, 121.
35. Choi, S. W.; Jo, S. M.; Lee, W. S.; Kim, Y.-R. Adv Mater 2003, 15, 2027.
36. Arora, P.; Zhang, Z. Chem Rev 2004, 104, 4419.